

High Resolution Millimeter Wave Imaging For Self-Driving Cars

Junfeng Guan, Sohrab Madani, Suraj Jog, Haitham Hassanieh
 Univeristy of Illinois at Urbana Champaign
 {jguan8, smadani2, sjog2, haitham}@illinois.edu

Abstract – Recent years have witnessed much interest in expanding the use of networking signals beyond communication to sensing, localization, robotics, and autonomous systems. This paper explores how we can leverage recent advances in 5G millimeter wave (mmWave) technology for imaging in self-driving cars. Specifically, the use of mmWave in 5G has led to the creation of compact phased arrays with hundreds of antenna elements that can be electronically steered. Such phased arrays can expand the use of mmWave beyond vehicular communications and simple ranging sensors to a full-fledged imaging system that enables self-driving cars to see through fog, smog, snow, etc.

Unfortunately, using mmWave signals for imaging in self-driving cars is challenging due to the very low resolution, the presence of fake artifacts resulting from multipath reflections and the absence of portions of the car due to specularly. This paper presents HawkEye, a system that can enable high resolution mmWave imaging in self driving cars. HawkEye addresses the above challenges by leveraging recent advances in deep learning known as Generative Adversarial Networks (GANs). HawkEye introduces a GAN architecture that is customized to mmWave imaging and builds a system that can significantly enhance the quality of mmWave images for self-driving cars.

1 INTRODUCTION

Self-Driving cars have generated a great deal of excitement. Last year, Tesla released a more affordable car model that supports automatic driving on highways and city streets and can respond to traffic lights and stop signs with a software update. More than 140,000 of these cars are already on the road [53]. Another company, Waymo, recently launched the first commercial self-driving taxi service in Arizona [41] and major car manufacturers like Toyota and Honda have invested up to \$3 billion in research and development on autonomous driving [7, 55, 57].

Despite this progress, the vision of fully autonomous vehicles, referred to as level 5 in the standards for driving automation, still remains a distant goal [14, 43, 44]. One of the major obstacles that the technology must overcome is its inability to function in inclement weather conditions such as fog, smog, snowstorms and sandstorms [11, 19, 56]. Autonomous

vehicles primarily use LiDARs or cameras to obtain an accurate and reliable view of the environment. However, since these sensors rely on optical frequencies for imaging, they suffer in low visibility conditions such as those caused by fog, snow and dust particles [34, 46, 47]. Cameras also suffer at night in low light conditions. This is problematic as many manufacturers including Tesla avoid using LiDAR altogether, making cameras their primary sensory module [54].

Millimeter wave (mmWave) wireless signals, on the other hand, offer far more favorable characteristics due to their ability to work at night and in inclement weather [13, 20]. This is why car manufacturers today use mmWave radar for the purpose of ranging, i.e., to determine the distance to other vehicles [5]. These radars, however, are limited to unidirectional ranging and cannot fully image the environment [9]. Luckily, the advent of 5G networks in the mmWave spectrum has led to the creation of compact phased arrays with hundreds of antennas [49, 72]. Such technology enables extremely narrow beams which can be steered electronically.

In this paper, we explore whether such 5G mmWave technology can extend beyond communication to enable full-fledged imaging in self-driving cars. In particular, by electronically steering the beam, one can capture reflections from different regions in space and potentially image the environment. Unfortunately, simply using very narrow steerable beams is not sufficient for three reasons:

- **Resolution:** While mmWave does offer higher resolution than standard wireless technologies, the spatial resolution is nowhere near what can be obtained from LiDARs or cameras. Fig. 1(c) shows an example of an image obtained from a high resolution mmWave system. The image appears as blobs of RF reflections and carries little to no contextual and perceptual information as opposed to a camera image and its corresponding 2D depth map shown in Fig. 1(a,b).
- **Specularity:** Wireless mmWave signals are highly specular i.e., the signals exhibit mirror-like reflections from the car [37]. As a result, not all reflections from the car propagate back to the mmWave receiver and major parts of the car do not appear in the image. This makes it almost impossible to detect the shape, size, and even orientation of the car as can be seen in Fig. 1(c).

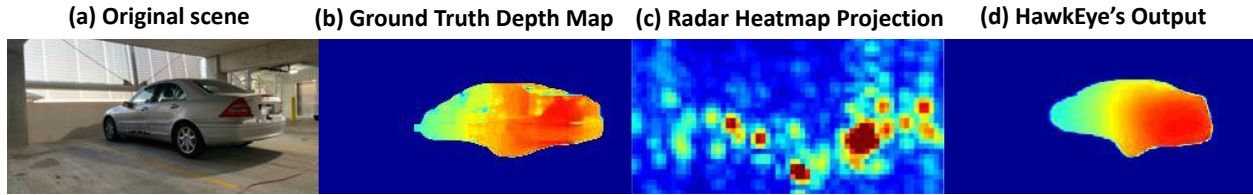


Figure 1: Specularity and Low Resolution in mmWave radar results in poor perceptual quality for images. To overcome this limitation, we exploit GAN architectures to create high resolution images from the low resolution mmWave radar heatmaps. The output from HawkEye is comparable to that captured from a stereo camera system.

- **Multipath:** Wireless reflections from the car can also bounce off the road and other cars and travel along multiple paths to the mmWave receiver creating shadow reflections in various locations in the scene as shown in Fig. 1(c). Hence, multipath can result in noisy artifacts in the image that are hard to interpret or dismiss as fictitious obstacles.

To address the above challenges, today’s commercial mmWave imaging systems, like airport scanners, use human-sized mechanically steerable arrays to improve the resolution. They also isolate the object being imaged in the near field to eliminate multipath and rotate the antennas around the object to address specularity [8, 38]. However, such a design would be extremely bulky and not practical for self-driving cars as we have no control over the cars being imaged.

In this paper, we introduce HawkEye, a system that can significantly improve the quality of mmWave imaging for self-driving cars by generating high resolution, accurate and perceptually interpretable images of cars from 3D mmWave heat-maps as shown in Fig. 1(d). To achieve this, HawkEye builds on a recent breakthrough in machine learning referred to as GANs (Generative Adversarial Networks). GAN is a learning paradigm that has proved to be a very effective tool for improving image resolution and generating realistic looking images [23, 35]. HawkEye trains a GAN using stereo depth maps obtained from camera images (as ground truth) to learn a mapping that increases the resolution, fills in the missing gaps due to specularity and eliminates artifacts caused by multipath. This allows HawkEye to estimate the location, shape, orientation, and size of the car in the scene.

Designing and training a GAN architecture that is capable of transforming 3D mmWave heatmaps to high resolution 2D depth maps poses new challenges beyond standard vision-based learning for image-to-image translation¹. Specifically, HawkEye addresses the following three challenges in adapting GANs to mmWave imaging.

1) Discrepancy in Perspective & Dimensions: HawkEye must learn to generate a high resolution 2D depth-map from a 3D mmWave heat-map. That is, HawkEye’s ground-truth

and output correspond to a 2D image with pixels corresponding to depth, while its input corresponds to a 3D image where every voxel value maps to RF signal strength. However, input and output in GANs are usually both 2D [62, 63, 69] or both 3D [30]. One solution to this discrepancy would be to transform the 2D depth maps to 3D point clouds where each voxel value maps to a binary one or zero, and use a point cloud GAN similar to [36] to generate 3D point clouds from 3D heat-maps. However, such a design results in very sparse high-dimensional output data. Training such a 3D GAN is known to be notoriously hard. It requires the network to learn significantly more parameters which exponentially increases the optimization search space making it difficult for the network to converge [52]. Instead, HawkEye separately encodes both the 2D input and 3D output into a common 1D space through separate neural networks (Fig. 4). This significantly reduces the complexity of the network [6] while also allowing for the direct comparison of encoded input and output, as will be discussed in detail in section 5.

2) Quantitative Accuracy: GANs have proven to be an extremely powerful tool for generating realistic images that are hard to distinguish from real life images [32]. However, HawkEye’s goal is not simply to generate a realistic looking car, but to also reconstruct the accurate shape, size, orientation, and location of the car from the mmWave heat-map. In order to ensure quantitative accuracy, we modify the loss function that the GAN aims to optimize. Specifically, instead of simply using the standard GAN loss, we add an L_1^2 loss term and a perceptual loss term to ensure the output is quantitatively and perceptually close to the ground-truth.

In addition to modifying the loss function, we also adapt the idea of *skip-connections* to our GAN. Specifically, *skip-connections* allow us to directly map features between the input and the output which are typically difficult for GANs to learn [45]. For example, mmWave provides very accurate ranging data which should be mapped directly to the output. Without such *skip-connections*, the GAN might degrade the accuracy of the car’s location. HawkEye adapts *skip-connections* to directly transfer such features from 3D input to 2D output.

¹This includes increasing resolution of a camera image, transforming black and white images to colored, transforming cartoon images to photo-realistic images, generating images with modified context, etc. [29, 60, 68]

² L_1 loss represents the absolute value of the difference between pixels in the output and ground-truth.

3) Training: Training GANs requires collecting thousands of data samples to ensure that the system generalizes well and does not overfit to the training data. However, collecting such a huge number of mmWave images on real cars takes a prohibitively long time. To address this, we start by training our GAN using synthesized mmWave images. We build a simulator to generate mmWave heatmaps from 3D CAD models of various car types. The simulator uses precise ray tracing models to capture the propagation and reflection characteristics of mmWave RF signals as well as specularities and artifacts resulting from multipath. After training with synthesized data, we fine tune the GAN using real data that we captured in order to create a more robust and reliable system. Finally, we test on real data that was not included in the training set using standard k -fold cross-validation.

Implementation & Evaluation: We implement HawkEye and empirically evaluate its performance on real mmWave images. We build a mmWave imaging module that uses FMCW waveform at 60 GHz and Synthetic Aperture Radar (SAR) to emulate a large antenna array for capturing 3D mmWave heatmaps of the scene. We collect 240 real images of 40 different car models from various viewpoints, distances and backgrounds. To evaluate HawkEye’s performance under different weather conditions, we also collect images in various visibility conditions ranging from clear visibility to different degrees of fog and rain. We summarize the results as follows:

- **Qualitative Results:** We provide several qualitative results similar to Fig. 1 in section 9.1. The results show that HawkEye is able to accurately recover the shape, size and orientation of the car from the mmWave input. We also show HawkEye’s performance in low visibility conditions like fog and rain, and demonstrate that HawkEye is able to recreate accurate images in such low visibility conditions and can generalize to different environments.
- **Quantitative Results:** We evaluate HawkEye by computing the error in its estimates of the location, orientation, shape, and size of the car. Our results show that HawkEye improves the accuracy of these estimates 2.2 – 5.5× compared to the 3D mmWave heatmaps .

Contribution: This paper has the following contributions:

- The paper presents the first system that can construct high resolution 2D depth maps of cars from noisy low resolution mmWave images. The system consists of four main components: a simulator that generates synthetic training data, a mmWave imaging system that captures real data, deep learning GAN architecture that reconstructs the output images, and a system for extracting quantitative measures such as size and orientation from the output.

- The paper presents a new GAN architecture that is tailored for mmWave imaging to account for perspective mismatch and quantitative accuracy.
- The paper demonstrates a working system that provides significant improvement in the quality of mmWave imaging for self-driving cars. It also demonstrates that the system can work in low visibility conditions like fog and rain through real test data points collected in such inclement weather conditions.

Limitations: HawkEye presents the first step towards high resolution imaging with mmWave wireless systems. However, HawkEye has a few limitations that are worth discussing. Notably, due to the lack of cheap, commercial phased arrays, our experimental setup uses SAR which precludes real-time frame capture. As phased array technology becomes more accessible in the coming years [49, 72], we plan to extend our platform to a real-time system. Another limitation is that our GAN was mainly trained on cars. We plan to extend it to pedestrians, bicycles and other road infrastructure in the future. We elaborate on these limitations in Section 10 and we propose future directions to address them.

2 RELATED WORK

(a) Sub-6 GHz Wireless Imaging Systems: Our paper is related to recent work on sub-6 GHz wireless imaging of the human body. The work aims to extract and track the human skeleton to estimate the 3D pose of the body [2, 66, 67]. It leverages human motion to combat specularities by combining reflections from different body parts over time and stitching them to form the full human body. [66, 67] also use deep convolutional neural networks to label various body parts and map them to 3D models of the human skeleton that can be tracked over time. Our work is different in two aspects. First, unlike humans in indoor settings, cars move as one single rigid body and only a single viewpoint of the car is typically observed in practice. Therefore, even during motion, most portions of the car will remain invisible to the system. Second, our goal is to generate higher resolution images rather than label different body parts in the RF image. To this end, we adopt a generative architecture (GAN), which is the state-of-the-art in image generation.

(b) Millimeter Wave Imaging Systems: Our work is also related to traditional mmWave imaging systems that can achieve high resolution [8, 21, 38, 48, 50]. These systems, however, only work in the near field ($< 50cm$), require huge amount of bandwidth ($> 10 GHz$) and use very bulky human-sized arrays similar to airport security scanners [8]. Other systems can achieve high resolution at longer distances using focal-plane arrays [4, 21, 39]. However, these require integrating optical components like a large focusing lens and a mechanically steerable raster. Hence, they are bulky

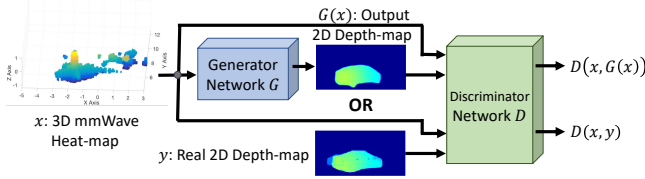


Figure 2: Conditional GAN Architecture.

and perform poorly on mobile platforms like self driving cars [50]. Finally, some radar applications use eigen-space image processing algorithms like MUSIC and ESPRIT to improve resolution [10, 27]. However, these techniques cannot deal with specularities and artifacts resulting from multipath. They also assume the signal sources are incoherent which is not the case in mmWave reflections.

More recent work uses commercial 60 GHz mmWave radars for imaging and tracking objects [61, 70, 71]. However, this work is limited to classifying the surface curvature of the object as concave or convex, localizing the object and tracking it in the 2D plane. The closest to our work are [1, 17]. [17] uses convolutional neural networks to create mmWave SAR images from a smaller SAR array. Similarly, [1] applies neural networks to radar acquisitions to enhance their resolution. Both [1, 17], however, use radar data both as input and ground-truth to their system, making them inherently incapable of dealing with challenges like specularities and multipath. Moreover, they both focus on short-range scenarios. HawkEye, in contrast, is a mmWave imaging system that can generate high resolution images in the far field ($> 10m$). HawkEye’s output recovers the visual representation of the cars and learns to cope with specularities and multipath.

(c) Super-Resolution & Image Transformation: In computer vision, neural networks are used to increase the resolution of camera images and near-Infrared images [22, 24, 35, 58]. Such techniques rely on the correspondence of image patches between low and high resolution images and can achieve an upscaling factor of $4\times$. Millimeter wave images, however, have significantly lower spatial resolution and some of the visual features like boundaries and edges are not apparent. GANs are also used to transform near-Infrared or low light images to visible images of the same resolution [12, 65]. In these applications, however, the images have the same resolution and share a significant amount of visual similarities. Finally, in addition to improving resolution, HawkEye addresses two challenges: missing portions of cars due to specular reflections and artifacts caused by multipath.

(d) LiDAR in Fog There is work on improving the performance of LiDAR in fog [34, 46, 47]. However, even state-of-the-art research systems either require knowing a depth map of the scene a priori [34] or work only when the object is static by estimating the statistical distribution of the photon reflected off the object [46, 47]. These systems also work

only up to 54 cm and have limited resolution (32×32 pixels) and field of view. Millimeter wave, on the other hand, can penetrate through fog, rain, and snow. Hence, mmWave radar can augment vision-based systems in self-driving cars to work in inclement weather.

3 PRIMER ON GANS

GANs are generative models that have proven to be very successful since they are able to generate data samples that closely follow the distribution of data without explicitly learning the distribution. To do so, GANs adopt an adversarial learning paradigm where two players compete against each other in a *minimax* game [23]. The first player, the Generator G , attempts to generate data samples that mimic the true distribution, e.g. generate realistic 2D depth-maps of cars. The second player, the Discriminator D , attempts to differentiate between samples generated by G from real data samples e.g. differentiate output of G from ground-truth 2D depth-maps from stereo cameras. G and D keep learning until G can generate samples that D can no longer distinguish from real samples of the true distribution. At this stage, D is no longer needed and G can be used during inference to generate new samples.

HawkEye uses a variant called conditional GANs (or cGANs) where G attempts to mimic a distribution of the data conditioned on some input [40], i.e. $P(y|x)$ where x is the low resolution mmWave heat-map and y is the high resolution 2D depth-map. x is given as input to both the generator G and the discriminator D . Fig. 2 shows the architecture of a conditional GAN. Intuitively, D serves two purposes. First, it helps generalize G by eliminating dependency on the environment i.e., G can create realistic images of cars by learning features that are independent of the background and location of the car in the training scenes. Second, it teaches G to fill in the missing parts of the car due to specularities and eliminate artifacts caused by multipath, i.e., unless artifacts are removed and specularities is addressed, D will be able to tell that the output was generated by G .

Mathematically, G learns a mapping from the input 3D mmWave heat-map x to the output 2D depth-map $G(x)$. D , on the other hand, attempts to learn a mapping from the input x and a 2D depth-map to a probability $\in [0, 1]$ of the 2D depth-map being real y , or generated $G(x)$. A perfect discriminator would give $D(x, y) = 1$ and $D(x, G(x)) = 0$. Hence, to win the game against a given G , D tries to maximize the following objective function:

$$\mathcal{L}(G) = \max_D \left(\mathbb{E}_y \left[\log D(x, y) \right] + \mathbb{E}_x \left[\log (1 - D(x, G(x))) \right] \right),$$

where the first term is maximized when $D(x, y) = 1$ and the second term is maximized when $D(x, G(x)) = 0$, i.e. when D correctly classifies the images as real or generated.

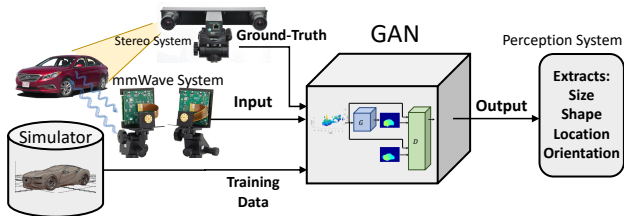


Figure 3: HawkEye’s System Overview.

G on the other hand tries to minimize the above objective function (which is referred to as its loss function $\mathcal{L}(G)$), since its goal is to fool the Discriminator into classifying its output data samples as being real. Therefore, the GAN optimization is a *minimax* problem given by:

$$\min_G \left(\max_D \left(\mathbb{E}_y [\log D(x, y)] + \mathbb{E}_x [\log (1 - D(x, G(x)))] \right) \right).$$

Since the mapping functions in G and D can be very complex, G and D are implemented and optimized using deep convolutional neural networks. The final output of the above GAN optimization is a G^* that minimizes the loss function $\mathcal{L}(G)$ and can be used to generate 2D depth-maps from new unseen 3D mmWave heatmaps. Few points are worth noting:

- The generator G never actually sees any real ground-truth data. Instead, it must learn to create realistic images based only feedback it receives from the discriminator D .
- The GAN never explicitly learns the distribution of the data. Prior to GANs, generative models would attempt to explicitly learn the distribution by approximating it as mixture of Gaussians or other simplified models that typically fail to capture the real distribution of data. GANs are very powerful since they can generate real looking samples without having to learn complex data distributions.
- The GAN adaptively learns its own loss function. Any machine learning model is trained by optimizing a given loss function that provides a quantitative measure of the model’s performance e.g. ℓ_1 or ℓ_2 distance. Choosing the right loss function is a very difficult task [29]. GANs are powerful since they do not require a fixed hand-tuned loss function and rather can adapt the loss function in the above equation as they learn.

4 SYSTEM OVERVIEW

HawkEye is a mmWave imaging system designed for autonomous vehicles. HawkEye can generate high resolution perceptually interpretable 2D depth-maps from 3D mmWave heat-maps. To do so, HawkEye has five modules shown in Fig. 3: a mmWave imaging module, a stereo camera, a simulator, a GAN, and a perception module. The stereo camera and simulator are used only during training and evaluation. The mmWave, GAN, and perception modules are used during training and testing. The perception system is also used

for evaluation by extracting metrics from the ground-truth, input and output. We summarize these components below:

- *GAN Architecture* (Sec. 5): We design a new GAN architecture customized for mmWave imaging in self-driving cars. The GAN uses an encoder-decoder paradigm, a modified loss function and skip connection to produce perceptually interpretable and accurate reconstructions of cars.
- *mmWave Imaging Module* (Sec. 6): We custom-build a mmWave imaging module using off-the-shelf 60 GHz radio and RF circuit components. It also uses a linear slider platform to emulate a large antenna array leveraging synthetic aperture radar, which provides us with more flexibility to test and experiment various parameters and setups. This module produces 3D mmWave heat-maps. However, on its own, it is intrinsically limited in resolution and suffers from specularly and artifacts caused by multipath.
- *Simulator* (Sec. 7): This module augments the training dataset with synthesized data obtained from 3D CAD models of cars and mmWave ray tracing algorithms. It produces both the ground truth 2D depth-map and the synthesized 3D mmWave depth-maps.
- *Stereo Camera* (Sec. 8): We custom-build a long-range stereo camera that can generate high-resolution 2D depth-maps of cars that serve as ground-truth for HawkEye.
- *Perception Module* (Sec. 9.2): This module allows us to extract quantitative metrics such as size, shape, location, orientation and boundary of the car. We use it to evaluate the output of HawkEye by comparing the output with the ground truth and the input mmWave 3D heat-maps.

Next, we will discuss these modules in more detail.

5 HAWKEYE’S GAN ARCHITECTURE

HawkEye leverages a cGAN architecture to enhance the resolution and quality of mmWave imaging in self-driving cars. However, unlike image-to-image mapping in computer vision, mmWave RF imaging brings in new challenges such as perspective mismatch between input and output, along with quantitative accuracy as described earlier. To address these challenges, HawkEye introduces a new GAN architecture tailored for mmWave imaging in self-driving cars.

HawkEye’s GAN must learn to generate a high-resolution 2D depth-map from a 3D mmWave heat-map. That is, HawkEye’s ground-truth and output are 2D images with each pixel representing depth, whereas its input is a 3D image where each voxel maps to RF signal strength. However, cGAN architectures typically map 2D input to 2D output [62, 63, 69] or 3D input to 3D output [30]. One solution to address the discrepancy in dimensions would be to transform the 2D

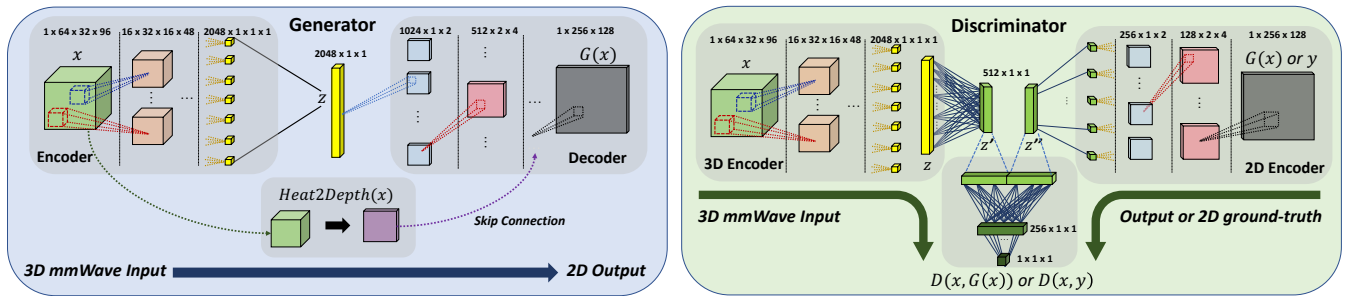


Figure 4: Network Architecture of the Generator G and Discriminator D .

depth-maps to 3D point clouds where each voxel value maps to a binary one or zero and use a point cloud GAN similar to [36] to generate 3D point clouds from 3D heat-maps.

Unfortunately, such design results in sparse high-dimensional input and output data. Training such 3D GAN is known to be notoriously hard [52]. As the sizes of the input and output increase, the number of parameters in the neural network of the generator G and discriminator D increase significantly. Consequently, the learning process that optimizes G and D must search through an exponentially larger space. Hence, it is more difficult for the network to converge and heuristics like gradient descent become more prone to getting stuck in local minima. For example, our input 3D heat-map x has a size of $64 \times 32 \times 96$. Increasing the resolution of the heat-map by $4\times$ would output a 3D point cloud $G(z)$ of size $256 \times 128 \times 384$. Training the neural network underlying G with this input and output size would require ≈ 10 billion parameters making the training intractable.

Instead, HawkEye first separately encodes both the 2D input and 3D output into a common 1D space through separate neural networks (Fig. 4). This design has two benefits. First, it significantly reduces the complexity of the network [6], and second, it allows for the encoded input and output to be compared directly. The resulting networks require ≈ 260 million parameters and can therefore be run on a standard GPU. Details of network design follow recommendations proposed in DCGAN [42].

A. Generator Architecture:

As described in section 3, the generator is implemented using deep neural networks. Following the previous paragraph, instead of directly generating the output from the input x using consecutive layers, the input is first encoded into a low-dimension representation z using an encoder network. z is then decoded into the output $G(x)$ using a decoder network. This type of structure is also known as the encoder-decoder architecture [6].

The vector z represents a common feature space between input and output. The input x represents the 3D mmWave heat-map in spherical coordinates (azimuth angle, elevation angle, range) generated by the mmWave module, where voxel

values represent the RF signal strength as we describe in more detail in section 6. The output $G(x)$ represents a higher resolution 2D depth-map where pixel values represent depth.

The encoder starts with one channel of 3D input. At each layer, there are 3D convolutions each of which is followed by Leaky-ReLU activation functions and batch-norm layers. With each layer, the number of channels increases and the size of the 3D kernel decreases until we get to an $n \times 1 \times 1 \times 1$ ($n = 2048$) vector z as shown in Fig. 4. z is then squeezed to an $n \times 1 \times 1$ vector to account for the dimension mismatch and passed to the decoder where it goes through the reverse process albeit using 2D transposed convolutions. Each layer in the decoder increases the size of the 2D kernel and decreases the number of channels until the output $G(x)$. In particular, the generator uses 5 convolutional layers in the encoder and 7 transposed convolutional layers in the decoder.

HawkEye’s generator also adapts the idea of *skip connections* between the encoder and the decoder [45]. Specifically, *skip connections* allow for information in an early layer to fast-forward directly to output layers. In our case, mmWave provides very accurate range information which, ideally, should be mapped directly to the output. As going through consecutive layers tends to saturate the accuracy of the approximation [26], we add a skip connection from input of the encoder to third-to-last layer of decoder.

Skip connections are generally implemented by simply concatenating output feature map of one layer to the input feature map of another layer of the same dimensions. However, in HawkEye’s architecture, none of the layers of the encoder and decoder have same dimension due to the dimension mismatch between the 3D input and 2D output. To address this, HawkEye introduces a heat-map to depth-map transformation. Specifically, for each 2D spatial location in the input 3D heat-map, we assign the depth as the location of the largest value (corresponding to highest signal strength) along the depth dimension. Formally,

$$x_{2D}(\phi, \theta) = \arg \max_r x_{3D}(\phi, \theta, r).$$

However, simply choosing the depth corresponding to the largest value is unstable and can lead to errors. Instead, we

choose the m largest values and create m channels of 2D depth-maps which we can then concatenate to a feature map of the same dimension in the decoder. It is worth noting that the above transformation only makes sense when applied to the input. We choose $n = 8$ in our implementation.

B. Discriminator Architecture:

The discriminator takes two inputs: the 3D mmWave heat-map x and a 2D depth-map that either comes from the ground-truth y or was generated $G(x)$. It outputs a probability of the input being real. In standard cGANs, the input and output of G typically have the same dimension. Hence, they are simply concatenated and fed as one input to D that uses a single deep neural network to output $D(x, y)$ or $D(x, G(x))$.

However, HawkEye’s input and output have different dimensions and hence cannot simply be concatenated and mixed together by one neural network. Instead, HawkEye uses two encoder networks inside the discriminator D as shown in Fig. 4. The first is a 3D encoder with the same architecture as that in the Generator. It outputs a low-dimension representation z . The second is a 2D encoder with 7 convolutional layers that takes the 2D depth-map y or $G(x)$ as input and outputs a low-dimension representation z'' . Before mixing the output of the two encoders, HawkEye ensures that they map to the same feature space by converting z to z' using a fully connected layer as shown in Fig. 4. z' and z'' are then concatenated and mapped to the output probability of the discriminator using two fully connected layers.

C. Loss Function:

The output of the discriminator D and generator G are used to calculate the loss function $\mathcal{L}(G)$ defined in section 3. During training, D and G are optimized to minimize this loss function. As mentioned earlier, GANs are very powerful at creating realistic images by capturing the high frequency components of the scene. However, they tend to be less accurate when it comes to low frequency components such as coarse object location, orientation, etc. The reason for this is that the objective of the generator G is to simply create high resolution images that look *real* to the discriminator D rather than accurate images with respect to metrics like location, orientation, etc. To address this, past work in machine learning manually adds an \mathcal{L}_1 loss term or a perceptual loss term \mathcal{L}_p [29, 31]. \mathcal{L}_1 loss is defined as the ℓ_1 distance between the ground truth and the output of the GAN (Eq. 1).

$$\mathcal{L}_1(G) = \mathbf{E}\|y - G(x)\|_1 \quad (1)$$

$$\mathcal{L}_p(G) = \mathbf{E}\|VGG(y) - VGG(G(x))\|_1 \quad (2)$$

$$\mathcal{L}_H(G) = \mathcal{L}(G) + \lambda_1 \mathcal{L}_1 + \lambda_p \mathcal{L}_p \quad (3)$$

For perceptual loss, a standard practice is to use a pre-trained network (e.g. VGG network from [51]) that extracts

perceptual features of the image. The ground truth and output are passed through this network and \mathcal{L}_p is computed as the ℓ_1 distance between the feature maps that the network outputs (Eq 2). The recent trend in computer vision is to avoid directly using \mathcal{L}_1 loss and instead use perceptual loss [31, 64]. This is because the difference between individual pixel values in images carries little to no perceptual information. Unlike images, pixel values in depth-maps correspond to depth and carry perceptual information about cars, such as orientation and shape. Hence, HawkEye maintains a combination of three losses (Eq. 3), where λ_1 and λ_p are hand-tuned relative weights of the loss functions. Using this loss function enables HawkEye to accurately capture both the low and high frequency components in the image. This results in perceptually interpretable high resolution images that faithfully represent the scene.

6 MMWAVE IMAGING MODULE

As described earlier, the advent of 5G in the mmWave spectrum has led to creation of electronically steerable phased arrays with hundreds of antenna elements [49, 72]. The very short wavelength of mmWave signals allows these phased arrays to have very small form factor. For example, at 60 GHz, a 32×32 array only occupies an $8cm \times 8cm$ patch.

Imaging: The ability to create very narrow beams and steer them electronically enables mmWave phased array radars to image 3D objects in the environment. Specifically, antenna array theory tells us that for $N \times N$ array, we can compute the reflected power along the spherical angles θ (elevation) and ϕ (azimuth) by adding a phase shift to the signal received on every antenna before combining the signals [33]. Formally,

$$x(\theta, \phi) = \sum_k^N \sum_l^N S_{k,l} e^{j \frac{2\pi}{\lambda} [(k-1)d \sin(\theta) \cos(\phi) + (l-1)d \cos(\theta)]}$$

where λ is the wavelength, $d = \lambda/2$ is the separation between consecutive elements, and $S_{k,l}$ is the signal received on the antenna element index by (k, l) in the 2D array.

The third dimension (the range ρ) is obtained by measuring the time of flight of the radar waveform echo. The huge bandwidth available in the mmWave band allows us to estimate range with high resolution. In our design we transmit a low power FMCW (Frequency Modulated Continuous Wave) similar to the one in [3], albeit at 60 GHz. We adopt a heterodyne architecture where we first generate the FMCW waveform at the baseband and then up-convert it to mmWave frequencies. The received signal is down-converted to baseband for radar waveform processing. This allows us to easily change the frequency band of operation to 24 GHz or 77 GHz by changing the mmWave front-end. The architecture is described in more details in section 8. The time of flight can be extracted from the FMCW using a simple FFT

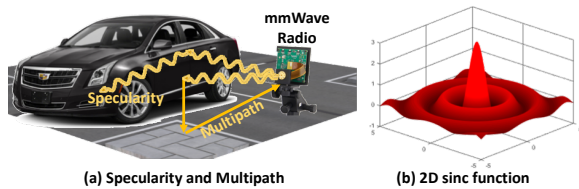


Figure 5: Challenges in mmWave Imaging

on the beat signal sampled below 1 MHz as described in [3]. This allows us to reconstruct a 3D heat-map $x(\theta, \phi, \rho)$.

Challenges: As described earlier, mmWave imaging suffers from 3 challenges. The first is resolution. The angular resolution is set by the size (aperture) of the antenna array and the range resolution is set by the bandwidth of the radar waveform. Specifically, for a bandwidth B , the range resolution is given by $\frac{c}{2B}$ where c is the speed of light. The range resolution for our system is 10 cm (with $B = 1.5$ GHz) which is $3.3\times$ worse than that of the commercial LiDAR [59].

Resolution along the other two dimensions, however, is significantly worse. The Rayleigh limit of the angular resolution is given by $\pi\lambda/L$ where L is the antenna aperture given by $L = N\lambda/2$ [33]. Even with the small antenna array form factor at mmWave frequency, we would need a 9 m long antenna array to achieve sub-degree angular resolution similar to LiDAR [59].³ Today’s practical mmWave systems have a much smaller (around $100\times$) aperture which limits the resolution, resulting in the image getting convolved with a very wide 2D sinc function similar to the one shown in Fig. 5 (b). That is why the mmWave image along the azimuth and elevation dimension mainly looks like blobs as shown in Fig. 1 (c) where most of the perceptual content such as object boundaries are lost.

Resolution, however, is not the only challenge. Unlike light, mmWave signals do not scatter as much and mainly reflect off surfaces. This leads to specularity as shown in Fig. 5 (a) where some reflections never trace back to the mmWave receiver, making certain portions of the car impossible to image. Moreover, due to multipath propagation, some reflections bounce off the street and other obstacles and trace back to the receiver as shown in Fig. 5 (a) creating many artifacts in the mmWave image as shown in Fig. 1 (c).

Synthetic Aperture Radar (SAR): Due to the limited availability of large 2D phased arrays in commercial systems, HawkEye emulates it using the synthetic aperture radar approach. As opposed to the analog beam-forming in phased array radars, we implement digital beam-forming at the receiver. We synthesize a large antenna array with a 60 GHz front-end and an FMCW baseband circuit, by physically scanning a single antenna element. The signal from each antenna

³Note that for systems like the airport security scanners, the target being imaged is in short range and hence, human sized arrays are sufficient.

element location is sampled, and phase-shifts are applied in digital afterwards. While this presents a limitation that prevents our implementation from operating in non-static scenarios, it gives us the flexibility to experiment with various array sizes. We discuss the implementation of SAR and this limitation in sections 8 and 10 respectively.

7 HAWKEYE’S DATA SIMULATOR

As mentioned earlier, the amount of data required to train our GAN is in the order of thousands of input and groundtruth images. Collecting such huge amount of data would take a prohibitively long time. To address this, we build a simulator that synthesizes paired up 3D mmWave heat-maps and 2D depth-maps of cars from 3D CAD models.

Our simulator is designed to create 3D point reflector models of cars and then simulate reflected mmWave signals using ray tracing. It takes into account multipath reflections as well as specularity based on reflection angles to generate realistic mmWave 3D heat-maps. The simulation has 3 stages:

- (1) *Scene generation:* We first simulate scenes of cars based on two types of datasets: 3D CAD model for an autonomous driving dataset [18] and Cityscapes [15], a street view video recordings dataset. The 3D CAD models provide us with precise 3D meshes of a wide variety of vehicles, while the street view photos offer references for car placement through object masks captured with Mask R-CNN [25].
- (2) *Ray Tracing:* Here we model the radar cross-sections of the scene. Occluded bodies are removed through spherical projection. Then, the radar cross-sections of the remaining surfaces are modeled as a cluster of point reflectors with different densities and reflectivities. We pinpoint corner areas with more scattering and specular surface areas whose reflection will not be received, and model point reflectors to perform standard ray tracing [16].
- (3) *Ground-truth & mmWave image generation:* We then simulate the received signal based on the point reflector model with background noise introduced. We add thermal noise to the FMCW signals and error in antenna element positions to better match the real data. By applying standard mmWave image processing as described in section 6 we get the 3D mmWave heat-map. The ground-truth 2D depth-map is generated through spherical projection of the 3D scene and coloring the pixels according to the depth.

8 IMPLEMENTATION

A. GAN Implementation & Training: The output of the discriminator and generator are used to calculate loss function $\mathcal{L}(H)$ as described in section 3. The generator and discriminator are trained end-to-end by optimizing the loss function. We follow the standard back-propagation algorithm and train on an Nvidia Titan RTX GPU.

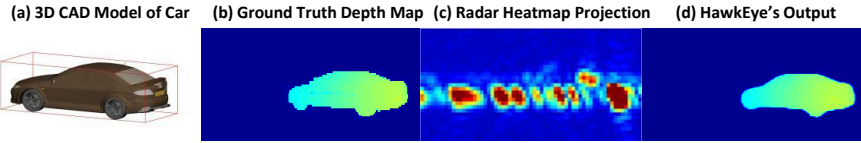


Figure 6: HawkEye's qualitative performance on synthetic test data.

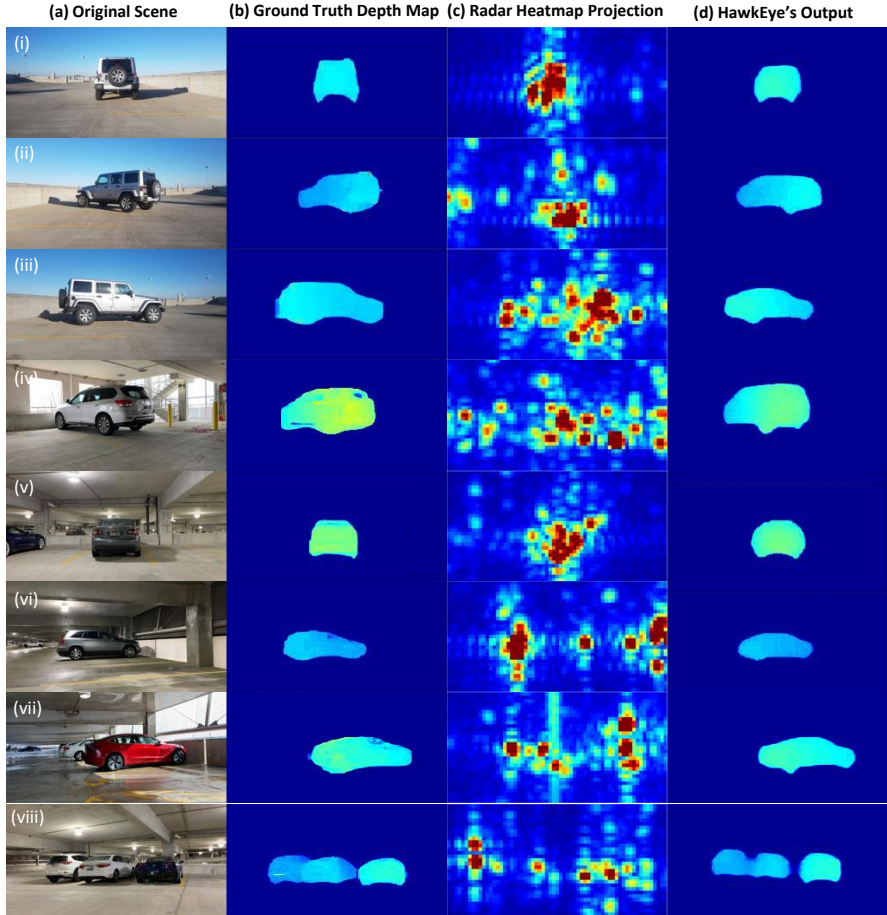


Figure 7: HawkEye's qualitative performance on real test data.

The training dataset is formed of 3000 synthesized images of cars with a batch size of 4. We use 120 different car models while varying the orientation and location of each car. After 170 epochs, we fine tune the GAN using 100 real mmWave images. We test on 500 synthesized images and 140 real images. In the test methodology, we follow standard k -fold cross-validation where $k = 5$. We ensure that the examples in the test dataset are not used during training. The real images come from 40 different car models with various orientations and locations.

B. mmWave Imaging: As described earlier the mmWave imaging radar comprises 60 GHz radios and SAR. For SAR, we build a 2D linear slider platform shown in Fig. 8 using three FUYU FSL40 linear sliders with sub-millimeter accuracy. A horizontal slider scans the mounted receiver antenna

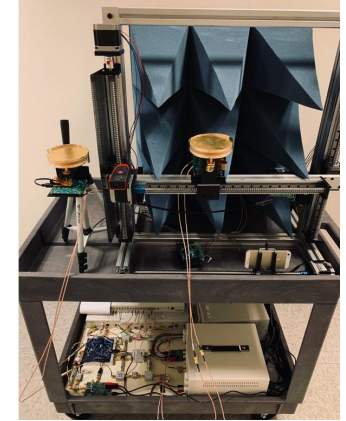
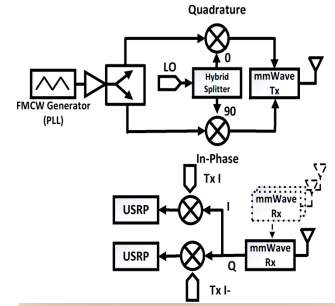


Figure 8: Millimeter Wave Platform

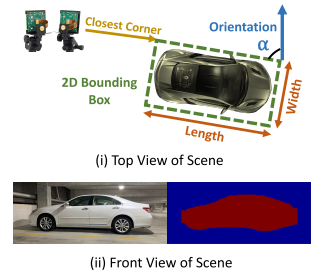


Figure 9: Metrics

along the X-axis, while two vertical sliders scan along the Z-axis. This platform allows us to synthesize a reconfigurable antenna array with a wide range of frequency and aperture. In HawkEye, only a fraction of $20\text{cm} \times 20\text{cm}$ area is scanned to emulate a 40×40 array at 60 GHz. The scanning time is 5 minutes, and will reduce to 90 seconds for a 20×20 array.

For the mmWave circuit, we implement a heterodyne architecture as shown in Fig. 8. We first generate the FMCW with triangular waveform at baseband, sweeping a bandwidth of 1.5 GHz. Then we up-convert it to 60 GHz with quadrature modulation using Pasternack 60 GHz radio frontend. The resulting signal after sideband suppression sweeps from 59.5 GHz to 61 GHz. In the receiver, we implement quadrature demodulation and sample the I and Q components of the complex signal with two synchronized USRPs for direct phase measurement and shifting.

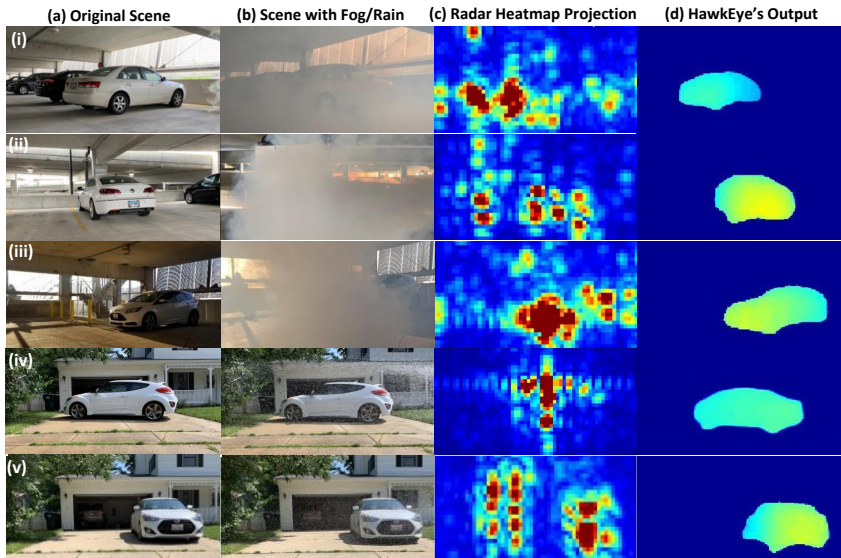


Figure 10: HawkEye’s performance with fog/rain in scene.

C. Stereo Camera & Generating Ground-truth: Ideally, we would use LiDAR to generate the ground-truth. However, LiDAR systems are extremely expensive and avoided by many autonomous car manufactures like Tesla. Hence, we opt for a stereo camera system to generate 2D depth-maps for our ground-truth. We place an iPhone X on a linear slider to capture multiple images of the scene. We then apply standard stereo image processing to extract the 2D depth-map. We filter out pixels that do not belong to the vehicles of interest using labeled object masks, that we create by applying a pre-trained labeled object detection model, Mask R-CNN [25] on raw camera images.

It is important to note that the mmWave imaging module and the stereo camera module, even when placed at the same location, will not yield the same view point and field of view. Hence, we calibrate for such discrepancy to be able to accurately train and test the GAN.

9 EVALUATION

We compare HawkEye against the ground truth obtained from the stereo camera system as well as images generated by the mmWave imaging system. *All evaluation is performed on outputs from the testing dataset that were not shown to the GAN during training.* We present both qualitative and quantitative results. The quantitative results are extracted using the perception module described in section 9.2.

9.1 Qualitative Results

We show HawkEye’s performance on the synthetic test data generated from our simulator in Fig. 6 and on real radar heat-maps captured in outdoor environments in Fig. 7. Column (a) shows the car being imaged (the license plates are

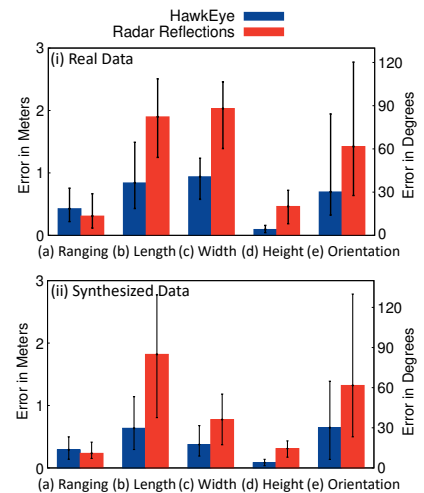


Figure 11: Quantitative Results.

blurred), and Column (b) shows the corresponding 2D stereo depth-map of the car. Columns (c) and (d) show the 2D front-view projection of the radar heat-map and the output of HawkEye respectively. We can see that HawkEye accurately reconstructs the shape and size of the car in the scene, and captures key defining features such as its wheels and orientation. HawkEye can also accurately determine the distance of the car in 3D space, as can be seen from the depth-maps.

These results show that even though the GAN was trained primarily on synthesized training data, it could generalize well to real data with only a small amount of fine-tuning during training. Hence, the simulator faithfully emulates the propagation characteristics of mmWave signals by using precise ray tracing models and incorporating other artifacts such as specular and multipath reflections.

Results in Fog/Rain: We also conduct experiments in fog and rain to test HawkEye’s performance in poor visibility conditions where today’s optical sensors fail. Due to practical limitations and to avoid the risk of water damage to our setup, we conduct controlled experiments where we emulate real fog and rain. We use a fog machine along with a high-density water-based fog fluid to emulate severe and realistic fog conditions. We emulate rain using a water hose in a confined region around the object of interest (the car).

It is important to note that HawkEye’s GAN model was never trained with examples collected in fog or rain. During training, HawkEye only uses synthetic data and is fine-tuned with real data collected in clear weather conditions. We present experimental results for fog (Fig.10 (i)-(iii)) and rain (Fig.10 (iv)-(v)). Column (a) and (b) show the original clear scene with the car, and the same scene with fog/rain respectively. Column (c) shows the 2D projection of the mmWave

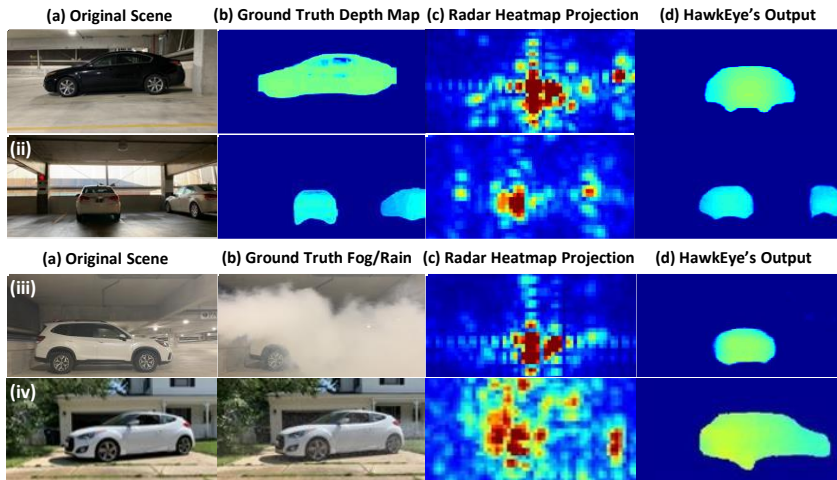


Figure 12: Examples where HawkEye fails.

radar heat-map captured in the scene with fog/rain, and Column (d) shows the corresponding output of HawkEye. From Fig.10, we can see that HawkEye can accurately reconstruct the car’s size and the 2D location, while preserving the key perceptive features such as orientation and shape.

While the fog and rain particles do introduce additional environmental reflections in the radar heat-map, our GAN model is able to ignore environmental reflections and extract out only the key generative features for the car in the scene. HawkEye’s ability to create accurate images in fog and rain, despite never having been trained with such examples, demonstrates that we can leverage the favorable propagation characteristics of mmWave signals in inclement weather conditions to build a model that can generalize well between different environments and weather conditions.

Failure Examples: Fig.12 shows some failure cases of HawkEye. A current limitation of our system is that its performance deteriorates when the scene has multiple cars (Fig.12(ii)). While HawkEye correctly identifies the number of cars in the scene, it makes errors in their shapes and relative locations. To address this, a potential future direction is to adopt a *Region Proposal Network*, similar to [67], where HawkEye can first isolate the reflections from each car in the scene, and then reconstruct the body of each car individually.

In Fig.12(iii) and (iv) we show failure cases with fog and rain respectively. It is worth noting that we are constrained to build our experimental setup at the 60 GHz unlicensed spectrum, which suffers from higher attenuation from water particles compared to other frequencies in the mmWave band. We believe that implementing HawkEye at the 77 GHz band, which is specifically allocated for automotive radar applications, will result in even better performance. HawkEye could also be specifically trained with images collected in bad weather to further improve the results.

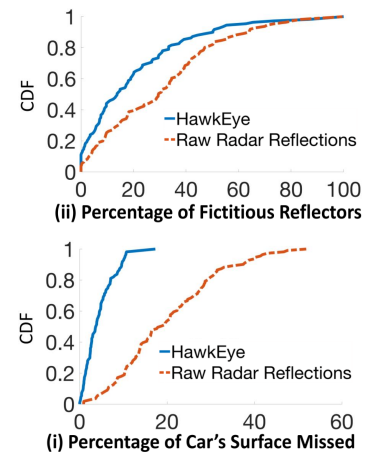


Figure 13: Accuracy of shape of car.

9.2 Quantitative Metrics

We leverage a perception module to extract the following quantitative metrics that correspond to the contextual and perceptual information in the scene as described below:

Ranging: We compare the ranging performance of HawkEye and radar to the ground truth. We assign the ranging distance to be the distance between the closest corner of the car and the radar imaging system in the 2D plane (Fig. 9(i)). We use the closest corner in our evaluation since the corners of the car scatter mmWave signals, and therefore, they can almost always be detected by the mmWave radar despite specular reflections from other parts of the car.

Size of Car: We evaluate the performance on estimation of size by comparing the accuracy in length, width and height of the car. For the 3D radar heat-map, we can measure the car dimensions as observed from the radar reflections. For the output from HawkEye, we can measure the dimensions by projecting the 2D depth-map into a 3D point cloud.

Orientation of Car: We measure the orientation as the angle between the longer edge of the car and the geographic north as viewed in the top view shown in Fig. 9(i). We can project the 2D depth-map or the 3D heat-map along the top view of the scene using standard rotational transformations.

Shape of Car: We evaluate the shape of the car by comparing the boundary of the car as viewed along the front-view, that is, along the view of the 2D depth-map (Fig. 9(ii)). We consider the following two metrics:

- *Percentage of the Car Surface Missed* — Indicative of the specularly effects observed in the image.
- *Percentage of Fictitious Reflectors* — Indicative of artifacts such as multipath and ambient reflections in the image.

9.3 Quantitative Results

In Fig. 11 we plot bar graphs depicting the performance of HawkEye and the mmWave radar on the metrics described in the previous subsection. In Fig. 11(i) we plot the results for the real test dataset, whereas in Fig. 11(ii) we plot the results for the synthetic test dataset. As can be observed, the results are similar for both and hereafter we will only discuss the results on the real dataset.

Ranging: In Fig. 11(i)(a), we plot the ranging error of the car. Due to the high sensing bandwidth at mmWave frequencies, mmWave radars can achieve high depth resolution. Therefore, mmWave radars can accurately detect the closest corner of the car with a median error of 30 cm. The skip connections in our design allow for direct transfer of this ranging information from input to output, allowing HawkEye to accurately range the car with a 42 cm median error.

Size of Car: From Fig. 11(i)(b,c,d), we see that mmWave radar has a median error of 1.9 meters, 2.1 meters and 0.47 meters in length, width and height respectively. In comparison, HawkEye achieves corresponding errors of 0.84 meters, 0.93 meters and 0.09 meters, offering a 2.26 \times , 2.26 \times and 5.22 \times improvement respectively. mmWave radars suffer from such large errors due to either specular reflections which lead to underestimation of the car dimensions, or artifacts such as multipath and environmental reflections which results in overestimation. However, HawkEye learns to fill in the holes in the radar heat-map to account for specularities and reject artifacts to only retain the true reflections from the car.

Orientation: Fig. 11(i)(e) shows the error in the estimated orientation of the car. As mentioned previously, we estimate the orientation from the top-view bounding box of the car. However, due to specularities and ghost reflections, the radar is unable to accurately estimate the bounding box and therefore leads to a large median error of 62 $^\circ$, whereas HawkEye achieves a median error of 30 $^\circ$.

Shape of Car: We evaluate the shape along two metrics:

- **Percentage of the Car Surface Missed** — Fig. 13(i) shows the CDF of the Percentage of the Car’s surface missed by the radar and HawkEye. This metric is similar to false negative rate with the 2D stereo camera depth-map as the ground truth. Due to specularities effects, most reflections from the car do not trace back to the receiver for the mmWave radar. As a result, mmWave radars miss a large portion of the car’s surface, with the median value of Percentage Missed being 30%. In comparison, HawkEye achieves a median value of 13%, thus showing that HawkEye can effectively learn to fill in the holes in the image and can accurately capture the surface of the car.
- **Percentage of Fictitious Reflectors** — Fig. 13(ii) shows the CDF of the Percentage of Fictitious Reflectors in the radar

and HawkEyeimage. This metric is similar to false positive rate. Radar heat-maps suffer from fictitious reflections due to artifacts such as multipath and environmental reflections, and as a result have a large number of false positives. In Fig. 13(ii), we can see that the median value for percentage of fictitious reflections for the radar is 20%, whereas the 90% percentile value is 38%. In comparison, HawkEye achieves a median value of 3.7% and a 90% percentile of 9.6%, resulting in an improvement of 5.5 \times and 4 \times respectively. This shows that HawkEye can effectively learn to reject the ghost reflections from the environment.

The above results show that HawkEye faithfully captures the shape of the car and reconstructs an accurate and high resolution image, consequently outperforming state-of-the-art mmWave radar systems as demonstrated in this section.

10 LIMITATIONS AND DISCUSSION

We have shown that HawkEye is a promising approach for achieving high resolution imaging with mmWave wireless systems, by leveraging the latest advancements in AI and machine learning. However, HawkEye has some limitations.

- **Real-time Implementation:** Our current implementation uses SAR to collect raw mmWave heat-maps. A more practical choice would be to use phased arrays that would enable realtime capture even as the cars are moving. However, this is infeasible due to the lack of cheap commercially available very large phased arrays today. As phased array technology becomes more accessible in the following years [49, 72], we plan to transform HawkEye to a realtime system that supports mobility. Note that Doppler shifts introduced by moving cars in the scene will not affect HawkEye’s performance, since we can easily estimate and correct for Doppler shifts using our triangular FMCW waveform, as is standard in radar signal processing [28].
- **Extending Beyond Cars:** We train HawkEye to specifically reconstruct cars. However, a practical system should extend to image pedestrians, bicycles, traffic signs, etc. One possibility is to adopt the approach from past work [67] where a separate classification network first isolates reflections from each class of objects, and then employs a separate GAN model to reconstruct the shape of each object. There is also scope to further improve the performance of our system with multiple cars in the scene.
- **Even Higher Resolution:** Our current system offers an upscaling factor of 4 \times in the size of the image. However, the actual increase in resolution is significantly higher as can be seen in the qualitative figures. We could potentially have larger upscaling factors but this would result in an exponentially higher amount of resource requirement in terms of memory, compute power and size of the training dataset beyond what GPUs can currently handle.

REFERENCES

- [1] Sherif Abdulatif, Karim Armanious, Fady Aziz, Urs Schneider, and Bin Yang. 2019. An Adversarial Super-Resolution Remedy for Radar Design Trade-offs. *arXiv preprint arXiv:1903.01392* (2019).
- [2] Fadel Adib, Chen-Yu Hsu, Hongzi Mao, Dina Katabi, and Fredo Durand. 2015. RF-Capture: Capturing the Human Figure Through a Wall. *ACM SIGGRAPH Asia* (2015).
- [3] Fadel Adib, Zach Kabelac, Dina Katabi, and Robert C Miller. 2014. 3D tracking via body radio reflections. *Proceedings of the 11th USENIX Conference on Networked Systems Design and Implementation (NSDI '14)* (2014).
- [4] Roger Appleby and Rupert N. Anderton. 2007. Millimeter-wave and submillimeter-wave imaging for security and surveillance. *Proc. IEEE* (2007).
- [5] Audi Technology Portal. 2019. Adaptive Cruise Control With Stop and Go Function. <https://www.audi-technology-portal.de/en/electrics-electronics/driver-assistant-systems/adaptive-cruise-control-with-stop-go-function>.
- [6] Vijay Badrinarayanan, Alex Kendall, and Roberto Cipolla. 2017. Segnet: A deep convolutional encoder-decoder architecture for image segmentation. *IEEE transactions on pattern analysis and machine intelligence* 39, 12 (2017), 2481–2495.
- [7] Bloomberg. *Press Release, 2018*. Autonomous-Car Tech Investment Skyrockets on SoftBank Deals.
- [8] Manufacturing Board. 2017. *Airport Passenger Screening Using Millimeter Wave Machines*.
- [9] BOSCH Inc. 2019. Adaptive Cruise Control. <https://www.bosch-mobility-solutions.com/en/products-and-services/passenger-cars-and-light-commercial-vehicles/driver-assistance-systems/adaptive-cruise-control/>.
- [10] Michael L. Burrows. 2004. Two-dimensional ESPRIT with tracking for radar imaging and feature extraction. *IEEE Transactions on Antennas and Propagation* (2004).
- [11] Bloomberg Businessweek. *Press Release, 2018*. Self-Driving Cars Can Handle Neither Rain nor Sleet nor Snow.
- [12] Chen Chen, Qifeng Chen, Jia Xu, and Vladlen Koltun. 2018. Learning to see in the dark. In *Proceedings of the IEEE Conference on Computer Vision and Pattern Recognition*. 3291–3300.
- [13] Chuan Cheng Chen. 1975. *Attenuation of electromagnetic radiation by haze, fog, clouds, and rain*. Technical Report. RAND CORP SANTA MONICA CA.
- [14] The Car Connection. *Press Release, 2018*. NHTSA regulator: Self-driving vehicles shouldn't be regulated – yet.
- [15] Marius Cordts, Mohamed Omran, Sebastian Ramos, Timo Rehfeld, Markus Enzweiler, Rodrigo Benenson, Uwe Franke, Stefan Roth, and Bernt Schiele. 2016. The cityscapes dataset for semantic urban scene understanding. In *Proceedings of the IEEE conference on computer vision and pattern recognition*. 3213–3223.
- [16] Vittorio Degli-Esposti, Franco Fuschini, Enrico M Vitucci, Marina Barbiroli, Marco Zoli, Li Tian, Xuefeng Yin, Diego Andres Dupleich, Robert Müller, Christian Schneider, et al. 2014. Ray-tracing-based mm-wave beamforming assessment. *IEEE Access* 2 (2014), 1314–1325.
- [17] Shiwei Fang and Shahriar Nirjon. 2018. AI-Enhanced 3D RF Representation Using Low-Cost mmWave Rada. In *ACM SenSys*.
- [18] Sanja Fidler, Sven Dickinson, and Raquel Urtasun. 2012. 3D Object Detection and Viewpoint Estimation with a Deformable 3D Cuboid Model. In *NIPS*.
- [19] Forbes. *Press Release, 2016*. How Autonomous Vehicles Will Navigate Bad Weather Remains Foggy.
- [20] Keegan Garcia, Mingjian Yan, and Alek Purkovic. 2018. Robust traffic and intersection monitoring using millimeter wave sensors. (2018).
- [21] Mohammad Tayeb Ghasr, Matthew J. Horst, Matthew R. Dvorsky, and Reza Zoughi. 2017. Wideband microwave camera for real-time 3-D imaging. *IEEE Transactions on Antennas and Propagation* (2017).
- [22] Daniel Glasner, Shai Bagon, and Michal Irani. 2009. Super-resolution from a single image. *Proceedings of the IEEE International Conference on Computer Vision* (2009).
- [23] Ian Goodfellow, Jean Pouget-Abadie, Mehdi Mirza, Bing Xu, David Warde-Farley, Sherjil Ozair, Aaron Courville, and Yoshua Bengio. 2014. Generative adversarial nets. In *Advances in neural information processing systems*. 2672–2680.
- [24] Axel-Christian Guei and Moulay Akhloufi. 2018. Deep learning enhancement of infrared face images using generative adversarial networks. *Applied optics* 57, 18 (2018), D98–D107.
- [25] Kaiming He, Georgia Gkioxari, Piotr Dollár, and Ross Girshick. 2017. Mask r-cnn. In *Proceedings of the IEEE international conference on computer vision*. 2961–2969.
- [26] Kaiming He, Xiangyu Zhang, Shaoqing Ren, and Jian Sun. 2016. Deep residual learning for image recognition. In *Proceedings of the IEEE conference on computer vision and pattern recognition*. 770–778.
- [27] P. Hoogeboom, F. Belfiori, and W. van Rossum. 2012. 2D-MUSIC technique applied to a coherent FMCW MIMO radar. *IET International Conference on Radar Systems (Radar 2012)* (2012).
- [28] Eugin Hyun, Woojin Oh, and Jong-Hun Lee. 2010. Two-step moving target detection algorithm for automotive 77 GHz FMCW radar. In *2010 IEEE 72nd Vehicular Technology Conference-Fall*. IEEE, 1–5.
- [29] Phillip Isola, Jun Yan Zhu, Tinghui Zhou, and Alexei A. Efros. 2017. Image-to-image translation with conditional adversarial networks. *Proceedings - 30th IEEE Conference on Computer Vision and Pattern Recognition, CVPR 2017* (2017).
- [30] Dakai Jin, Ziyue Xu, Youbao Tang, Adam P Harrison, and Daniel J Mollura. 2018. Ct-realistic lung nodule simulation from 3d conditional generative adversarial networks for robust lung segmentation. In *International Conference on Medical Image Computing and Computer-Assisted Intervention*. Springer, 732–740.
- [31] Justin Johnson, Alexandre Alahi, and Li Fei-Fei. 2016. Perceptual losses for real-time style transfer and super-resolution. In *European conference on computer vision*. Springer, 694–711.
- [32] Tero Karras, Samuli Laine, and Timo Aila. 2018. A Style-Based Generator Architecture for Generative Adversarial Networks. *CoRR* abs/1812.04948 (2018). [arXiv:1812.04948](http://arxiv.org/abs/1812.04948) <http://arxiv.org/abs/1812.04948>
- [33] Hamid Krim and Mats Viberg. 1996. Two Decades of Array Signal Processing Research. *IEEE Signal Processing Magazine* (1996).
- [34] Martin Laurenzis, Frank Christnacher, Emmanuel Bacher, Nicolas Metzger, Stéphane Schertzer, and Thomas Scholz. 2011. New approaches of three-dimensional range-gated imaging in scattering environments. In *Electro-Optical Remote Sensing, Photonic Technologies, and Applications V*, Vol. 8186. International Society for Optics and Photonics, 818603.
- [35] Christian Ledig, Lucas Theis, Ferenc Huszár, Jose Caballero, Andrew Cunningham, Alejandro Acosta, Andrew Aitken, Alykhan Tejani, Johannes Totz, Zehan Wang, and Wenzhe Shi. 2017. Photo-realistic single image super-resolution using a generative adversarial network. *Proceedings - 30th IEEE Conference on Computer Vision and Pattern Recognition, CVPR 2017* (2017).
- [36] Chun-Liang Li, Manzil Zaheer, Yang Zhang, Barnabás Póczos, and Ruslan Salakhutdinov. 2018. Point Cloud GAN. *CoRR* abs/1810.05795 (2018). [arXiv:1810.05795](http://arxiv.org/abs/1810.05795) <http://arxiv.org/abs/1810.05795>
- [37] Jonathan S Lu, Patrick Cabrol, Daniel Steinbach, and Ravikumar V Pragada. 2013. Measurement and characterization of various outdoor 60 GHz diffracted and scattered paths. In *MILCOM 2013-2013 IEEE Military Communications Conference*. IEEE, 1238–1243.

- [38] B. Mamandipoor, G. Malysa, A. Arbabian, U. Madhow, and K. Noujeim. 2015. 60 GHz synthetic aperture radar for short-range imaging: Theory and experiments. *Conference Record - Asilomar Conference on Signals, Systems and Computers* (2015).
- [39] Yang Meng, Anyong Qing, Chuan Lin, Jiefeng Zang, Yizhe Zhao, and Cheng Zhang. 2018. Passive Millimeter Wave Imaging System Based on Helical Scanning. *Scientific Reports* (2018).
- [40] Mehdi Mirza and Simon Osindero. 2014. Conditional generative adversarial nets. *arXiv preprint arXiv:1411.1784* (2014).
- [41] The Washington Post. *Press Release, 2018*. Waymo launches nation's first commercial self-driving taxi service in Arizona.
- [42] Alec Radford, Luke Metz, and Soumith Chintala. 2015. Unsupervised representation learning with deep convolutional generative adversarial networks. *arXiv preprint arXiv:1511.06434* (2015).
- [43] MIT Technology Review. *Press Release, 2016*. What to Know Before You Get In a Self-driving Car.
- [44] MIT Technology Review. *Press Release, 2018*. Uber is right to rethink its self-driving operations.
- [45] Olaf Ronneberger, Philipp Fischer, and Thomas Brox. 2015. U-net: Convolutional networks for biomedical image segmentation. In *International Conference on Medical image computing and computer-assisted intervention*. Springer, 234–241.
- [46] Guy Satat, Barmak Heshmat, Dan Raviv, and Ramesh Raskar. 2016. All Photons Imaging Through Volumetric Scattering. *Scientific Reports* (2016).
- [47] Guy Satat, Matthew Tancik, and Ramesh Raskar. 2018. Towards photography through realistic fog. In *2018 IEEE International Conference on Computational Photography (ICCP)*. IEEE, 1–10.
- [48] T Savelyev, Zhuge Xiaodong, B Yang, A Yarovoy, L Lighthart, M Drozdov, and B Levitas. 2010. Development of UWB microwave array radar for concealed weapon detection. *Radar Symposium (IRS), 2010 11th International* (2010).
- [49] Shahriar Shahramian, Michael J. Holyoak, Amit Singh, and Yves Baeyens. 2019. A Fully Integrated 384-Element, 16-Tile, W-Band Phased Array With Self-Alignment and Self-Test. *IEEE Journal of Solid-State Circuits* (2019).
- [50] David M. Sheen, Douglas L. McMakin, and Thomas E. Hall. 2007. Near field imaging at microwave and millimeter wave frequencies. *IEEE MTT-S International Microwave Symposium Digest* (2007).
- [51] Karen Simonyan and Andrew Zisserman. 2014. Very deep convolutional networks for large-scale image recognition. *arXiv preprint arXiv:1409.1556* (2014).
- [52] Edward Smith and David Meger. 2017. Improved adversarial systems for 3d object generation and reconstruction. *arXiv preprint arXiv:1707.09557* (2017).
- [53] Tesla Inc. 2018. Tesla Fourth Quarter and Full Year 2018 Update. <http://ir.tesla.com/static-files/0b913415-467d-4c0d-be4c-9225c2cb0ae0>.
- [54] Tesla Inc. 2019. Autopilot | Tesla. <https://www.tesla.com/autopilot>.
- [55] ThomasNet. *Press Release, 2018*. Toyota Makes 500 Million USD Investment in Self-Driving Cars.
- [56] The New York Times. *Press Release, 2016*. 5 Things That Give Self-Driving Cars Headaches.
- [57] The New York Times. *Press Release, 2018*. Honda to invest 2.75 billion USD in GM's Cruise autonomous vehicle unit.
- [58] Yusuke Tomoto. 2016. Chainer implementation of "Perceptual Losses for Real-Time Style Transfer and Super-Resolution". *Arxiv* (2016).
- [59] Velodyne. [n.d.]. Velodyne Lidar Ultra Puck Datasheet. ([n. d.]), 2–3.
- [60] Ting-Chun Wang, Ming-Yu Liu, Jun-Yan Zhu, Andrew Tao, Jan Kautz, and Bryan Catanzaro. 2018. High-resolution image synthesis and semantic manipulation with conditional gans. In *Proceedings of the IEEE Conference on Computer Vision and Pattern Recognition*. 8798–8807.
- [61] Teng Wei and Xinyu Zhang. 2015. mTrack: High-Precision Passive Tracking Using Millimeter Wave Radios. *Proceedings of the 21st Annual International Conference on Mobile Computing and Networking (ACM MobiCom '15)* (2015).
- [62] Donggeun Yoo, Namil Kim, Sunggyun Park, Anthony S Paek, and In So Kweon. 2016. Pixel-level domain transfer. In *European Conference on Computer Vision*. Springer, 517–532.
- [63] He Zhang, Vishwanath Sindagi, and Vishal M Patel. 2017. Image de-raining using a conditional generative adversarial network. *arXiv preprint arXiv:1701.05957* (2017).
- [64] Richard Zhang, Phillip Isola, Alexei A Efros, Eli Shechtman, and Oliver Wang. 2018. The unreasonable effectiveness of deep features as a perceptual metric. In *Proceedings of the IEEE Conference on Computer Vision and Pattern Recognition*. 586–595.
- [65] Teng Zhang, Arnold Wiliem, Siqi Yang, and Brian Lovell. 2018. TV-GAN: Generative adversarial network based thermal to visible face recognition. *Proceedings - 2018 International Conference on Biometrics, ICB 2018* (2018).
- [66] Mingmin Zhao, Tianhong Li, Mohammad Abu Alsheikh, Yonglong Tian, Hang Zhao, Antonio Torralba, and Dina Katabi. 2018. Through-wall human pose estimation using radio signals. *Cvpr* (2018).
- [67] Mingmin Zhao, Yonglong Tian, Hang Zhao, Mohammad Abu Alsheikh, Tianhong Li, Rumien Hristov, Zachary Kabelac, Dina Katabi, and Antonio Torralba. 2018. RF-based 3D skeletons. *Proceedings of the 2018 Conference of the ACM Special Interest Group on Data Communication - SIGCOMM '18* (2018). <http://dl.acm.org/citation.cfm?doid=3230543.3230579>
- [68] Jun Yan Zhu, Taesung Park, Phillip Isola, and Alexei A. Efros. 2017. Unpaired Image-to-Image Translation Using Cycle-Consistent Adversarial Networks. *Proceedings of the IEEE International Conference on Computer Vision* (2017).
- [69] Jun-Yan Zhu, Richard Zhang, Deepak Pathak, Trevor Darrell, Alexei A Efros, Oliver Wang, and Eli Shechtman. 2017. Toward multimodal image-to-image translation. In *Advances in Neural Information Processing Systems*. 465–476.
- [70] Yibo Zhu, Yanzi Zhu, Zengbin Zhang, Ben Y. Zhao, and Haitao Zheng. 2015. 60GHz Mobile Imaging Radar. *Proceedings of the 16th International Workshop on Mobile Computing Systems and Applications - HotMobile '15* (2015).
- [71] Yanzi Zhu, Yibo Zhu, Ben Y. Zhao, and Haitao Zheng. 2015. Reusing 60GHz Radios for Mobile Radar Imaging. *Proceedings of the 21st Annual International Conference on Mobile Computing and Networking - MobiCom '15* (2015).
- [72] Samet Zehir, Ozan Dogan Gurbuz, Arjun Kar-Roy, Sanjay Raman, and Gabriel M Rebeiz. 2016. 60-GHz 64-and 256-elements wafer-scale phased-array transmitters using full-reticle and subreticle stitching techniques. *IEEE Transactions on Microwave Theory and Techniques* 64, 12 (2016), 4701–4719.